

## A NUMERICAL EXPLORATION OF WEAKLY DISSIPATIVE TWO-DIMENSIONAL MAPS

**Carles Simó**

Departament de Matemàtica Aplicada i Anàlisi  
Universitat de Barcelona  
Spain  
carles@maia.ub.es

**Arturo Vieiro**

Departament de Matemàtica Aplicada i Anàlisi  
Universitat de Barcelona  
Spain  
vieiro@maia.ub.es

### Abstract

The aim of this work is to study the global dynamics of a planar weakly dissipative map around a perturbation of an elliptic fixed point. If the dissipative perturbation is assumed to be radial the map presents different domains depending on the topological behaviour. When showing these main domains the different  $\omega$ -limits that can co-exist are also described. Furthermore, the parametric study of the mechanism of destruction of resonances and the evolution of invariant objects of the phase space are displayed. On the other hand, the probability of capture in different kinds of resonances as a function of the parameters of the map and the dissipation parameter is also given. The numerical approach to these ideas provides a first step to develop a global theory for this kind of maps. In order to exhibit the generic properties of weakly dissipative maps a radially dissipative version of the Hénon map is considered.

### Key words

resonances, splitting of separatrices, twist map approximations, weakly dissipative global behaviour

### 1 Introduction

The main purpose of this work is to describe the global dynamics of a planar weakly dissipative map around an elliptic fixed point, that is, to understand global bifurcations, not only local ones, and  $\omega$ -limit sets. It is not a restriction to assume that the elliptic fixed point is located at the origin. We focus our attention on describing the creation and destruction of resonances and the position of the invariant manifolds associated to them when a radial dissipation is assumed to be added to the system. A numerical study is carried out in order to understand how the chaotic dynamics associated to these phenomena is created as well as to describe the behaviour of the probability of capture as a function of the dissipation parameter. Note, however, that the analysis in case of very small dissipation can only be done by analytic

tools because the number of iterates becomes too large: the global transport is too slow.

In order to guide a subsequent theoretical research about this topic an easy version of a weakly dissipation has been chosen. To be precise, a radial dissipation, depending linearly on the radial coordinate around the elliptic fixed point, is applied over the conservative dynamical system as a small perturbation. The numerical approach given in this note provides a good basis of a priori knowledge about this kind of systems.

The type of maps considered shares properties of the conservative and the dissipative cases. We show the existence of regions where the map has homoclinic points, regions where these points are destroyed, and how the resonances change their topology. Moreover, there is a region where the resonances disappear. Observe that no KAM curves remain when a dissipation effect is added to the system.

To illustrate the global behaviour of weakly dissipative maps by numerical experiments a mild dissipation of the classical Hénon map,

$$H_{\alpha,\epsilon}(x, y) = (1 - \epsilon)H_{\alpha}(x, y), \quad (1)$$

where

$$H_{\alpha} : \begin{pmatrix} x \\ y \end{pmatrix} \mapsto R_{2\pi\alpha} \begin{pmatrix} x \\ y - x^2 \end{pmatrix}, \quad (2)$$

has been chosen as a paradigmatic example. Nevertheless, the properties that are going to be displayed can be generalized to a generic weakly dissipative map with radial dissipation.

The choice of this map as an example is motivated by the role it plays to describe the dynamics around a saddle-node bifurcation (see [Broer, Roussarie and Simó, 1996]). In fact, up to order 2, generically, after a suitable rescaling of variables, the Hénon map is obtained in a neighbourhood of the saddle-node bifurca-

tion point. As it is going to be emphasized a saddle-node bifurcation is related to the existence of resonances. It is important also to recall that Hénon map is the simplest planar map with non trivial dynamics and that any other quadratic map with an stable fixed point can be reduced to it by a change of variables.

The Hénon map (2) has two fixed points: the origin  $E = (0, 0)$ , which is an elliptic fixed point, and the point  $P_h = (2 \tan \pi \alpha, 2 \tan^2 \pi \alpha)$ , which is a hyperbolic one. It is important to take into account that the Hénon map is reversible with respect to the axis  $y = \tan(\pi \alpha)x$  and also with respect the parabola  $y = x^2/2$  by means of the involutions  $(x, y) \mapsto (\cos(2\pi\alpha)x + \sin(2\pi\alpha)y, \cos(2\pi\alpha)x - \sin(2\pi\alpha)y)$ ,  $(x, y) \mapsto (x, x^2 - y)$ , respectively. The reader is referred to [Hénon, 1969] to get information about the properties of the Hénon map.

This note is organised as follows. Next section is a review of the conservative case while the third one deals with the problem of describing global dynamics of a weakly dissipative map. Finally, the last one concerns about resonances without homoclinic points (flow type resonances) and describes how the position of the invariant manifolds of the hyperbolic points of a periodic orbit in a concrete resonance changes the probability of capture. We close with a conclusion.

## 2 Review of the conservative case

The dynamics of a weakly dissipative map, despite of the dissipation effect, keeps a lot of properties of conservative systems. This section is devoted to sum up some well known facts of a discrete system generated by an area preserving map (APM) around an elliptic fixed point.

1) *Integrable APM.* An area preserving diffeomorphism is called *integrable* if there exists an autonomous Hamiltonian flow such that the time  $\tau$  map coincides with the diffeomorphism.

Resonances, which are characterised by the sequence of islands that form it, can appear. In particular, an island contains an elliptic periodic orbit. A hyperbolic periodic one appears at the boundary of the island. More concretely, the boundaries of the islands are the separatrices of the hyperbolic points.

It can be observed that the separatrices act as barriers between two kinds of different motions: librational motion and rotational motion. Around each island of the resonance the phase portrait is topologically equivalent to the one of a classical pendulum.

2) *Splitting of separatrices.* When the integrability is lost the properties above mentioned no longer hold. As it is known the splitting of the separatrices provides a beautiful structure where homoclinic points appear and the manifolds form a kind of trellis.

Generically, the intersection between the stable and unstable invariant manifolds (separatrices) is transversal and the angle formed is a measure of the splitting produced. The manifolds form then loops which are

mapped one to each other preserving area and orientation. The homoclinic tangle is also a geometrical way to understand how chaos is born in the system. The phase portrait around each island of a resonance is like the one of a periodically perturbed pendulum. The classical Hénon map (2) is an easy example of a non integrable APM.

3) *Invariant curves and resonances.* For a generic close to integrable APM the domains between resonances contain rotational invariant curves. It is important to recall that the rotation number over them is irrational while, on the other hand, rational rotation number corresponds to a resonance. In particular, the set of values of rotation number corresponding to resonances is of zero measure but dense.

4) *Last invariant curve.* Generically, the structure defined by invariant curves and resonances holds up to any hyperbolicity destroys it. The Hénon map (2) has a source of hyperbolicity on the invariant manifolds of the hyperbolic point  $P_h$ . To obtain the distance where is expected to have the “last” invariant curve, the dynamics along the separatrices close to the hyperbolic point has to be modelled, for instance, by means of the separatrix map

$$\begin{pmatrix} u \\ v \end{pmatrix} \mapsto \begin{pmatrix} u' \\ v' \end{pmatrix} = \begin{pmatrix} u + \alpha + \beta \log(v') \\ v + \sin(2\pi u) \end{pmatrix} \quad (3)$$

with  $(u, v) \in [0, 1) \times \mathbb{R}$ ,  $\beta = 1/\log \lambda$ , being  $\lambda$  the eigenvalue of modulus greater than one of the differential of the map at  $P_h$ , and where  $\alpha$  is a constant which includes the effect of the amplitude of the oscillations of  $W^u$  with respect to  $W^s$ . But, if the distance from the hyperbolic point is considered to be large (after suitable scalings), the separatrix map (3) can be rescaled ( $v = v_0 + s$ ,  $v_0$  relatively large) to obtain, approximately, the standard map

$$\begin{pmatrix} u \\ s \end{pmatrix} \mapsto \begin{pmatrix} u' \\ s' \end{pmatrix} = \begin{pmatrix} u + \hat{\alpha} + ks' \\ s + \sin(2\pi u) \end{pmatrix}, \quad (4)$$

where  $\hat{\alpha} = \alpha + \beta \log(v_0)$  and  $k = \beta/v_0$ . It is known that the last invariant curve for the standard map (4) is destroyed when  $k = k^* \approx 0.96/2\pi$  (see [Greene, 1979], [Olvera and Simó, 1987]). Then, the separatrix map has invariant curves if  $v_0 > \beta/k^*$ . By using a first order approximation of the passage of the invariant curve close to the hyperbolic point, the distance from the hyperbolic point to the region where we expect to have an invariant curve is given by  $d = \sqrt{\beta/k^*}$ . Moreover, the map (4) has the point  $(1/2, 0)$  as an elliptic point for  $k < 2/\pi$ . Denoting by  $\bar{k}$  this value, the distance at which we expect to find islands is given by  $d = \sqrt{\beta/\bar{k}}$ . We recall that in the expression of these distances  $\beta$  has been rescaled by the amplitude of the splitting.

5) *Birkhoff normal form.* The local dynamics near the elliptic fixed point can be studied by means of Birkhoff normal form. This provides a good approximation up to certain distance from the elliptic fixed point and the resonance structure is reflected on it. Generically, two types of resonances are found in the normal form: unavoidable resonances and resonances due to the closeness of the rotation number at the fixed point to a rational number. The second type are responsible of the islands that can be observed in the phase space. The other ones produce the twist effect.

6) *Twist condition and splitting.* Generically, in a small domain around the elliptic fixed point the rotation number is a monotone function with respect the radial coordinate. That is, a generic twist condition holds in a neighbourhood of the fixed point. However, far from this one the twist condition could be violated. Figure 1 shows the rotation number of the Hénon map for  $\alpha \in [0, 0.5]$ , scaled with step 0.01, as a function of the distance to the origin. The distance between the hyperbolic and elliptic fixed points of the map is scaled to be constant equal to one.

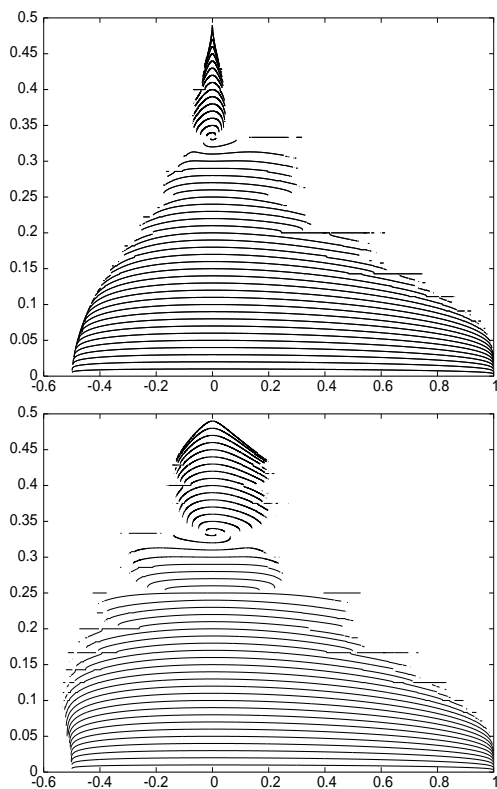


Figure 1. Representation of the rotation number ( $y$ -axis) as a function of the (normalized) distance to the origin ( $x$ -axis) for different values of  $\alpha$  (see text). The top one is obtained by taking initial points on the symmetry axis  $y = \tan(\pi\alpha)x$  while in the bottom one they are taken on the curve  $y = \frac{x^2}{2}$ .

In particular, it is observed in figure 1 that the derivative of the rotation number with respect the radial coordinate

is negative for small values of  $\alpha$  while changes its sign for values close to  $1/3$ . In the last case, the map loses its twist condition in such a form that the second derivative is positive as can be observed by the presence of maxima.

Usually, the information that can be obtained about the torsion of a map is restricted to interpretations of numerical results as above. Nevertheless, the model considered is extremely simple and analytical computation of normal form can be carried out. It is found, in such a way, that the first Birkhoff coefficient of the Hénon map is equal to zero only for  $\alpha_0 \approx 0.29021531163$ . Moreover,  $b_1$  is positive for values  $\alpha \in (0, \alpha_0)$  and negative otherwise. The second Birkhoff coefficient is zero for  $\alpha_1 \approx 0.2308206101$ ,  $\alpha_2 \approx 0.3137515644$  and  $\alpha_3 \approx 0.3944381765$ . Reference [Dullin, Meiss and Sterling, 1999] describes the behaviour of the first and second Birkhoff coefficients for the Hénon map.

We are interested in the splitting of the separatrices associated to the main hyperbolic periodic orbit of a resonance.

In general, for a generic *APM* the inner splitting (located closer to the elliptic fixed point at the origin) is different from the outer one. To decide which one is larger one has to look at the first two derivatives of the rotation number (of an integrable approximation) with respect to the radial coordinate, that is, to the torsion of the map and its first derivative (see [Simó and Vieiro, in progress]).

7) *Meandering curves.* Close to the radius where the twist condition is lost, typically, there is a creation of meandering curves (see [Simó, 1998]). For instance, taking  $\alpha \approx 0.3$  there are two periodic orbits of period 10. One of them is located in the region where the derivative of the rotation number with respect the radius is positive and the other where it is negative. For  $\alpha = 0.299545$  it is observed how a meandering curve is going to be created. Figure 2 shows the meandering curve obtained for  $\alpha = 0.299544$ . Moving the parameter  $\alpha$  to be  $\alpha = 0.299543$  the invariant curve is destroyed.

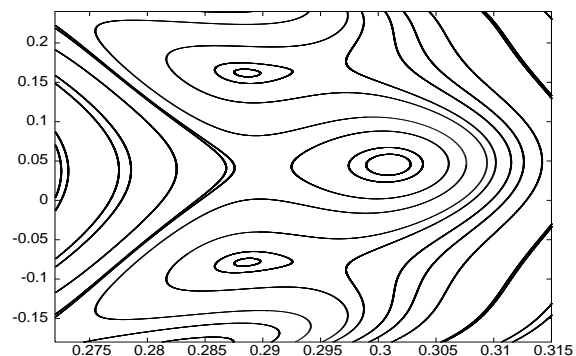


Figure 2. Meandering curve found when the twist condition is lost for  $\alpha = 0.299544$ .

As was said before, the splitting depends on properties of the torsion of the map. In particular, meandering curves appear in the region of the phase space where the splitting changes, generically, its behaviour.

### 3 The global behaviour of a radial weakly dissipative map

This section is devoted to understand how is the resonance structure of a weakly dissipative map depending on the dissipation parameter. Along this section a radial dissipative perturbation is assumed on the system. For numerical examples we consider the map (1) of the introduction.

The effect of the dissipation produces a displacement on the invariant manifolds of the conservative case. This change can affect a resonance in two different ways: the homoclinic points of the resonance could disappear or the resonance itself could be destroyed.

Observe that the elliptic fixed point of an area preserving map  $T$  becomes an stable focus due to the dissipation. Elliptic points inside the resonances change its topological appearance in the same way. Moreover, in Birkhoff normal form coordinates the elliptic and hyperbolic points of period  $m$  of a resonance close to the fixed point are located on two nearby concentric circumferences. The evolution of the fixed points of  $T^m$  with respect to the dissipation parameter is like rotations in different senses. They collide over a limit circumference where the points collapse and the resonance is destroyed as a result of a saddle-node bifurcation.

#### 3.1 Existence of resonances: first critical radius

An accurate analysis of the figure 1 provides us with qualitative information about the shape of resonances in the phase space. It is observed that taking  $\alpha$  close to zero the system seems to be integrable as it is noticed by the existence of invariant curves close to the hyperbolic point. Furthermore, no resonance is detected by the numerical method. When crossing a resonance through an island, as the rotation number  $\rho$  is rational, one should observe the corresponding horizontal line. Crossing the resonance through a hyperbolic point one should observe sudden changes of  $\rho$  of the typical form  $-1/\log d$  where  $d$  is the distance to the hyperbolic periodic point. Of course, close enough to the hyperbolic point the chaotic behaviour prevents to compute even an approximation of the rotation number. In particular, this means that the resonances are very small in this region ( $\alpha$  close to zero) and, consequently, the effect of the dissipation could destroy them.

The robustness of a resonance under the dissipation effect depends on the order and the amplitude of the resonance. It can be proved that the amplitude, in turn, depends on the order and on the distance to the elliptic fixed point where the resonance is located. Moreover, the distance at which it is located depends on the properties of the angle of the rotation around the ellip-

tic point (Diophantine conditions) as can be explained theoretically (see [Simó and Vei-ro, in progress]).

In order to clarify the effect of the dissipation on the resonances table 1 shows, for  $\alpha = 0.15$ , how the corresponding resonances are destroyed when the dissipation parameter increases. The disposition of the resonances in the phase space is depicted in figure 3. It is observed, as was stated before, that the destruction of the resonances depends not only on its position but on its amplitude. For instance, resonance (2:19) disappears before than resonance (1:7) which is located closer to the elliptic point.

$\log_{10}(\epsilon)$	Resonances destroyed
-6	All inside $B_0(0.27)$
-4.569	(2:19)
-4.625	(1:7)
-3.456	(1:8)
-3.297	(1:9)

Table 1. Considering  $\alpha = 0.15$  fixed, the table contains the values of the dissipation parameter  $\epsilon$  that correspond to a destruction of a resonance.

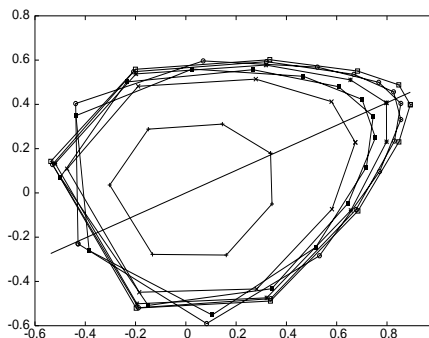


Figure 3. Location of the resonances (1:7), (1:8), (2:17), (1:9), (2:19) and (1:10) in the phase space (conservative case). The points correspond to the elliptic points inside each island and the lines join the points which are in the same resonance.

The example above shows the existence of a radius, depending on  $\epsilon$ , such that inside it no resonance survives under the dissipation effect. It can be proved for a generic radial weakly dissipative map the existence of such a radius. We call it the first critical radius,  $r_*$ , which differentiates qualitative different behaviours of the map. Inside it all points have as a  $\omega$ -limit the perturbed elliptic point while, outside the ball of radius  $r_*$ , some resonances survive and points could be captured by the stable foci inside them.

A full theoretical description can be found in [Simó and Vei-ro, in progress]. In particular, the theoretical

approach confirms the general idea explained above. By computing normal form around the fixed elliptic point of a conservative generic map, considering an approximation by a flow and adding the dissipative perturbation, it can be obtained the following equation which defines the first critical radius,

$$\log \epsilon > \frac{m-2}{2} \tilde{C} - \tau \left( \frac{m-2}{2} \right) \log m. \quad (5)$$

Constants  $\tilde{C}$  and  $\tau$  are related with the Diophantine conditions of  $\alpha$ . Constant  $c$  depends also on coefficients of the Birkhoff normal form around the origin. From the above equation, it can be obtained the minimum order of a resonance that is not destroyed,  $m$ . Then,  $r_* \approx \sqrt{2c/m^\tau}$  defines an approximation of the critical radius.

### 3.2 The role of the splitting of the conservative case: second critical radius

Assuming  $\epsilon$  fixed, outside the domain where the dissipation destroys the resonances, a finite number of them survive. Their shape depends on the effect of the dissipation over them. Namely, it is important to distinguish between the case when no homoclinic points exist and when some of them survive the dissipation.

Figure 4 illustrates how homoclinic points are destroyed by the dissipation effect. Also it can be observed that different types of trellises are found in this kind of maps.

Resonances with homoclinic points are found relatively far from the focus fixed point. For a fixed  $\epsilon$  there is a second critical radius,  $r_{**}$ , such that in the annulus of radii  $r_*$  and  $r_{**}$  some resonances survive but they do not have homoclinic structure. It is clear that if homoclinic points do not exist the dynamics around the resonance is like the one generated by a flow, that is a pendulum with torque. This case will be studied in detail in the next section.

Figure 5 shows the evolution of a resonance with respect the dissipation parameter  $\epsilon$ . For  $\epsilon$  small the island is like a periodically perturbed pendulum (1.). Then, for  $\epsilon$  greater the evolution of the island produces another outer splitting (2.). Increasing the parameter the outer one is broken and the other splitting produces a change on the shape of the resonance (3.). Finally, the effect of dissipation destroys the splitting and the resonance is a flow type one, like the one that generates a pendulum with torque (4.). We remark that this is one of the possible scenarios of the evolution of the effect of dissipation. If the inner splitting is larger than the outer one it would be different.

Let  $H_+$  and  $H_-$  be two consecutive hyperbolic periodic points of the same resonance strip and let  $W_+^u$ ,  $W_+^s$ ,  $W_-^u$  and  $W_-^s$  be the branches of the unstable and the stable manifolds associated to the points  $H_+$  and  $H_-$ , respectively. In order to clarify the scenario shown above table 2 contains the possible situations in the

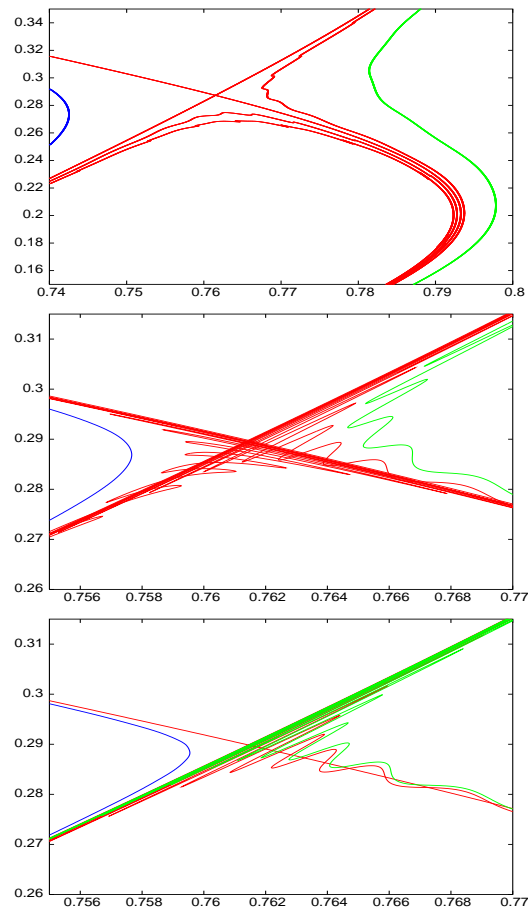


Figure 4. From top to bottom, the invariant manifolds close to a hyperbolic point of the (1:7) resonance for  $\alpha = 0.17$  and  $\log(\epsilon) = -4, -5.6$ , and  $-6$ , respectively, are represented.

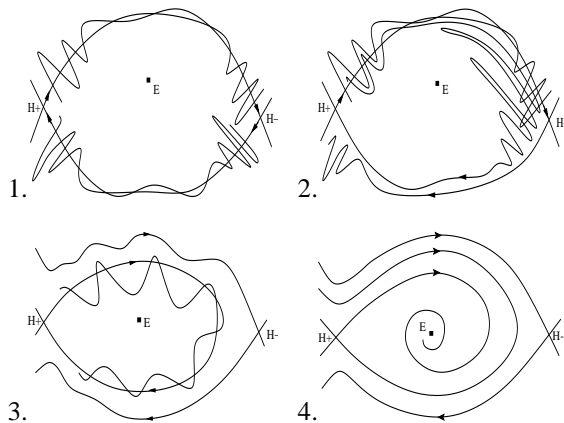


Figure 5. Scheme of a flow type resonance. The domain of attraction is clearly determined by the position of the invariant manifolds of the hyperbolic points of the resonance.

evolution of the resonance. It contains also the tangencies that produce different shapes on the resonance and that correspond to  $\epsilon = \epsilon_1, \epsilon_2$ , and  $\epsilon_3$ . It is remarkable the existence of an impossible tangency transition as it is noted in the table.

For  $\epsilon$  fixed, a resonance is of flow type or has homo-

$\epsilon$	0	> 0	(*)	$\epsilon_1$		$\epsilon_2$		$\epsilon_3$	great
$W_+^u, W_-^s$	i	i	i	i	i	t	-	-	-
$W_+^u, W_+^s$	i	i	i	i	i	i	i	t	-
$W_-^u, W_-^s$	i	i	t or -	-	-	-	-	-	-
$W_+^u, W_-^s$	i	i	i	t	-	-	-	-	-
Figure 5		1.			2.		3.		4.

Table 2. Possible situations of the invariant manifolds associated to two consecutive hyperbolic points  $H_+$  and  $H_-$  of the resonance. In the table “i” means that we have transversal intersection and “t” that the two corresponding manifolds have homoclinic tangency. The symbol “-” denote that no intersection between the manifolds exists. Observe that the positions (\*) are impossible to achieve. Last file is the correspondence with figure 5.

clinic points depending on both splittings of the conservative case, the inner one and the outer one, which, as was stated before, are generically different. Figure 6 shows the decimal logarithm of both splittings for the resonance (1:7). It corresponds to the Hénon map (2) for different values of  $\alpha$  for which the resonance exists and is not very small. The angle of the splitting is measured on the symmetry axis  $y = \tan(\pi\alpha)x$  where it is located the elliptic point of the resonance. Numerical evidence seems to predict that for most of the values of  $\alpha$  the outer splitting is bigger than the inner one. Moreover, at least in a first order approximation, this fact does not depend on the resonance considered as it is shown in figure 7. Note that this depend on the properties of the Hénon map, and can change if a different APM is considered. Nevertheless, we need to thoroughly examine the splitting of the conservative case in order to clarify what is observed.

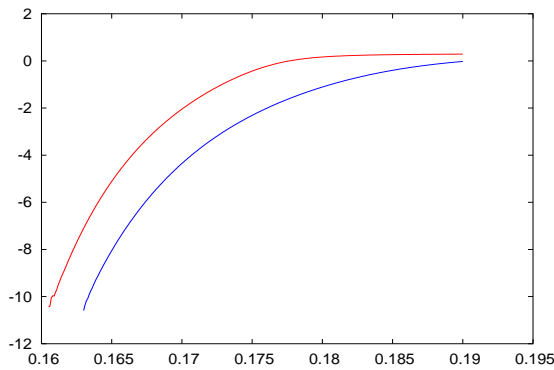


Figure 6. It is represented, on the vertical axis, the decimal logarithm of the splitting of the resonance (1:7), and on the horizontal one the value of  $\alpha$ . Red line corresponds to the outer splitting while blue line to the inner one.

Indeed, for a general diffeomorphism it is not necessarily true that the outer splitting is the bigger one. In

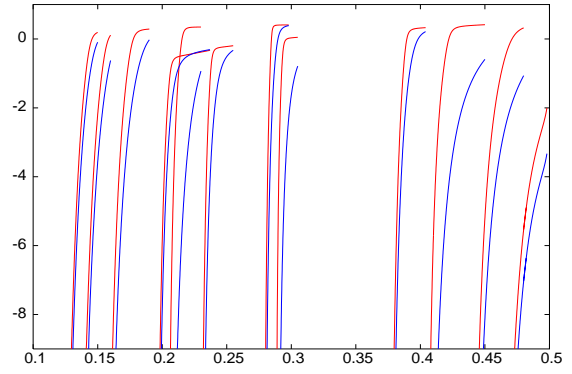


Figure 7. From left to right, it is represented the decimal logarithm of the splitting of the resonances (1:9), (1:8), (1:7), (2:11), (1:5), (2:9), (3:10), (2:7), (3:8), (2:5), (3:7) and (4:9), respectively. Each pair of red and blue lines corresponds to the outer splitting an inner splitting, respectively, of a different resonance.

fact, this is a property depending on the derivatives of the rotation number (of a nearby integrable map) with respect to the radial coordinate as was stated before and it is illustrated by the following example.

Consider an integrable twist map expressed in Poincaré coordinates

$$T : \begin{pmatrix} I \\ \theta \end{pmatrix} \mapsto \begin{pmatrix} I \\ \theta + \alpha(I) \end{pmatrix}, \quad (6)$$

where  $(I, \theta) \in (0, 1) \times (0, 2\pi)$ . Assume  $\alpha(I) = b_0 + b_1 I + b_2 I^2$ , that is, only the first and the second Birkhoff coefficients are different from zero. Let  $G$  denote the generating function associated to  $T$ ,

$$G(\hat{\theta}, I) = \hat{\theta} I - S(I), \quad (7)$$

where  $S(I) = -b_0 I - (b_1/2)I^2 - (b_2/3)I^3$ . By perturbation of the generating function

$$\tilde{G}(\hat{\theta}, I) = \hat{\theta} I - S(I) + \epsilon \sin \hat{\theta}, \quad (8)$$

we construct a non-integrable map close to  $T$

$$T_\epsilon : \begin{pmatrix} I \\ \theta \end{pmatrix} \mapsto \begin{pmatrix} I + \epsilon \cos(\theta + \alpha(I)) \\ \theta + \alpha(I) \end{pmatrix}. \quad (9)$$

Figure 8 displays the invariant manifolds for the (1:2) resonance for different values of the parameters of the model. It is observed that for some values the inner splitting is greater than the outer one and how changing torsion coefficients the inner becomes less than the outer one.

By theoretical approach, following reference [Fontich and Simó, 1990], generic upper bounds of the splitting could be obtained. They depend on the derivatives of

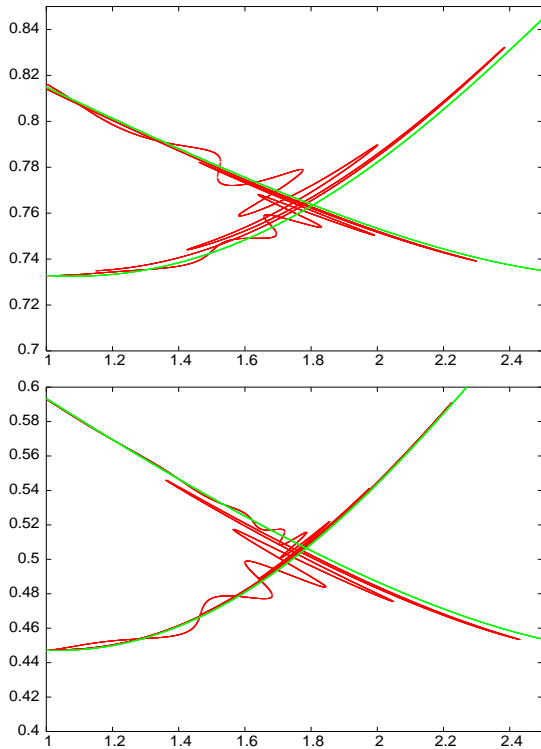


Figure 8. Different splittings observed for the model (9). We have chosen  $b_0 = 0$ . For the top picture  $b_1 = 0.2$ ,  $b_2 = 4$  and  $\epsilon = 0.14$ . The bottom one is obtained choosing  $b_1 = 6$ ,  $b_2 = -2$  and  $\epsilon = 0.14$ .

the rotation number with respect to the radial coordinate which agrees with what is observed numerically. For instance, the theory confirms that for the Hénon map it is easier to observe the outer splitting bigger than the inner one and, also, that this is due to the fact that the first and the second Birkhoff coefficients have the same sign for most of the values of  $\alpha$  (see section 2).

#### 4 Behaviour in the flow type domain

This section contains information on the probability of capture in a flow type resonance. The numerical approach helps us to understand geometrically how the capture is produced when the dissipation parameter is varied.

There is also an interest in studying the map very close to the conservative case. Observe that, for  $\epsilon = 0$ , the set of points with  $\omega$ -limit the origin,  $E$ , has Lebesgue measure 0. On the other hand, for  $\epsilon > 0$ , if we restrict the domain around the elliptic fixed point where initial points are considered to be finite, it has finite positive measure. The problem of finding which is the limit of this measure when  $\epsilon \rightarrow 0$  is also discussed along this section.

In a more specific way, let  $\mathcal{C}$  be a rotational invariant curve of the conservative map and let  $\mathcal{A}$  be the set of points located inside the invariant curve. Consider the

set

$$\Gamma(F, \epsilon) = \{(x, y) \in \mathcal{A} \mid \omega(x, y) = E\}, \quad (10)$$

for a generic weakly dissipative map  $F$ . Then, the limit behaviour to understand can be expressed as

$$\lim_{\epsilon \rightarrow 0} \mu(\epsilon) = \lim_{\epsilon \rightarrow 0} \frac{mes_L(\Gamma(F, \epsilon))}{mes_L(\mathcal{A})}, \quad (11)$$

where  $mes_L$  is the usual Lebesgue measure of  $\mathbb{R}^2$ . The value of the limit depends on the diffeomorphism considered and on the invariant curve  $\mathcal{C}$ .

We conjecture that the probability of capture in a resonance when  $\epsilon$  tends to zero is the measure of the islands of the resonances of the conservative case plus the measure of the strips that formed the invariant manifolds. Despite of the amplitude of the strips is close to zero when  $\epsilon$  is very small, the strips accumulate spiralling around the resonance strip giving rise, on a small ring around the resonance, to a set which has positive Lebesgue measure and which has a positive limit when  $\epsilon \rightarrow 0$ .

#### 4.1 The structure of the separatrices

As it was observed before the probability of capture by a resonance depends on the position of the invariant manifolds of the hyperbolic points. In fact, they bound an entrance strip and an exit strip for each island. Points between the stable manifolds of the same hyperbolic periodic point are those that will be captured by the island, that is, they tend to the periodic focus which has replaced the elliptic point of the resonance. In particular, the measure of the set of points with  $\omega$ -limit such a focus depends on the amplitude of the entrance strips (see figure 5 (4.)). Moreover, it can be observed that the amplitude of the entrance strip is not constant and increases when approaching, spiralling, to the island where it lands. On the other hand, points between the stable manifolds of different successive hyperbolic periodic points will be expelled from the resonance.

It is not easy to understand how these strips travel away through the phase space as predicts the existence of points far from the resonance that are captured by it. This means that the invariant manifolds of a hyperbolic point of the resonance must cross other resonances which implies the existence of heteroclinic orbits connecting both resonances.

Figure 9 shows how the strips of the eight order resonance (red) are folded before crossing the nine order resonance (blue). We see how the stable manifolds of a hyperbolic point of the resonance (1:8) must intersect with one of the unstable manifolds of the hyperbolic points of the resonance (1:9). In the same way, the unstable invariant manifold of the hyperbolic point of the resonance (1:9) folds when crossing the islands of the resonance (1:8) embracing each island and intersecting

the stable manifolds that constitute the exit strip. In particular, a horseshoe is created and, consequently, to determine the  $\omega$ -limit of a point of the phase space can be hard because of the sensitivity to initial conditions.

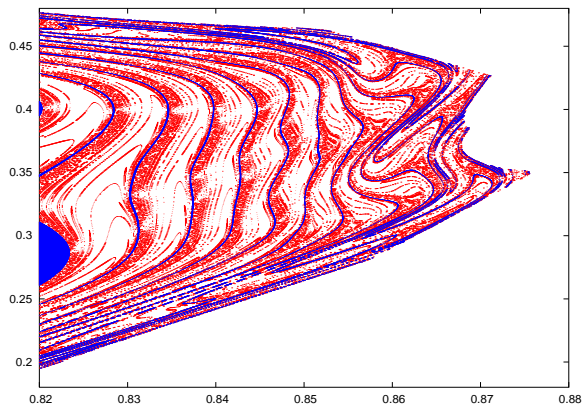


Figure 9. Folds of the stable invariant manifolds associated to the hyperbolic points of the (1:8) resonance (red) when crossing the resonance (1:9) (blue) for the Hénon map ( $\alpha = 0.15$ ,  $\epsilon = 10^{-4}$ ).

#### 4.2 Measure of the set with $\omega$ -limit the fixed point

This subsection is devoted to illustrate the behaviour of the limit (11) for values of  $\epsilon$  going to zero. The limit, as was observed before, depends on the map and on the dissipation parameter. On the other hand, we have shown before how complicated structure provides the way of pass through a resonance. Nevertheless, a numerical approach let us to understand the probability of travelling through all the resonances.

In order to get information about the probability of being captured by the fixed point at the origin and not for any stable focus of any resonance we iterate a set of points over the reversibility axis of the Hénon map. Some points, the closest ones to the hyperbolic fixed point, escape under iteration far from the neighbourhood of the focus fixed point at the origin following the invariant manifolds of the hyperbolic fixed point. The other points, the ones which remain inside a ball around the focus fixed point at the origin, could be captured by a resonance or could go through them to be captured by the origin. Figure 10 shows the ratio of the number of points that are captured by a resonance and the points that do not leave the neighbourhood of the origin.

The number of points that leave the stable domain due to the local hyperbolicity provided by the unstable manifolds of the hyperbolic point depends on the map considered. That is, it depends on the parameter  $\alpha$ . Figure 11 shows the ratio of the number of points that are captured in one resonance and the total of iterated points.

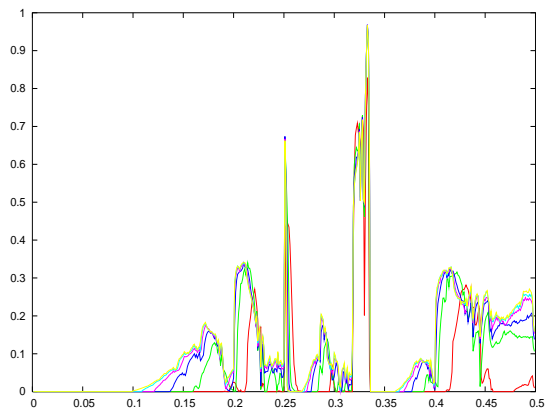


Figure 10. Ratio of the number of points with  $\omega$ -limit a focus of a resonance and the number of points inside the stable domain. On the  $x$ -axis is represented the parameter  $\alpha$  which defines the Hénon map. The different curves are obtained for different values of  $\epsilon$ :  $10^{-2}$  (red line),  $10^{-3}$  (green line),  $10^{-4}$  (blue line),  $10^{-5}$  (violet line),  $10^{-6}$  (sky blue line) and  $10^{-7}$  (yellow line).

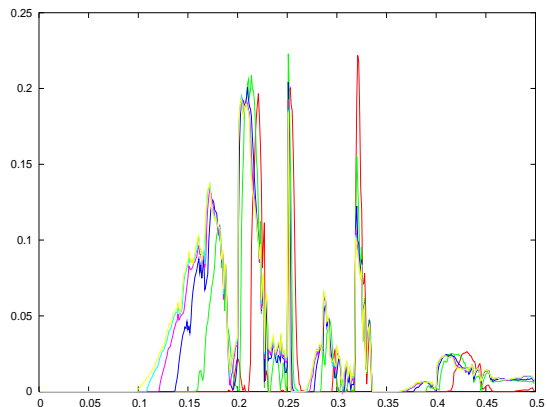


Figure 11. Ratio of the number of points with  $\omega$ -limit a focus of a resonance and the total number of iterated points. On the  $x$ -axis is represented the parameter  $\alpha$  which defines the Hénon map. The values of  $\epsilon$  used and the pattern of colours are the same as in figure 10.

A theoretical approach allows us to study the limit (11) for the flow domain (see [Simó and Vieiro, in progress]), that is, if we restrict the study to the ball of centre the origin and radius the second critical radius  $r_{**}$  (see section 3.2). In fact, neglecting the effect of other resonances different from the main one, which we assume to be the  $(q:m)$  resonance, for a generic map such that the rotation number at the origin is  $\alpha = q/m + \delta$ , we find that the limit of the probability of capture in the resonance when  $\epsilon$  tends to zero is of order  $\mathcal{O}(\delta^{\frac{m}{4}-1})$ . This conclusion seems to back the conjecture given before because if the resonance in the conservative case is assumed to be of a flow type the probability of capture must be equal to 0.

## 5 Conclusion

Hamiltonian dynamics is usually the first common approach to real world. However, weakly dissipative dynamics provides sometimes a more accurate approach to describe physical phenomena since effects like friction or medium resistance could be included in the model as small dissipative perturbations. In this sense, the present work examines which structures from the conservative case remain and how topology changes.

We have displayed the main properties of weakly area preserving maps by means of a very simple model. In particular, domains where the map shows topologically different behaviour have been determined. Inside each domain a different analytical approach has to be adopted in order to obtain both qualitative and quantitative information. The Birkhoff normal form around the elliptic point is the general model to consider.

Flow type resonances can be understood by means of flow approximation of the normal form as was briefly explained before. Nevertheless, when the resonances have homoclinic points flow approximation of the normal form cannot be considered and one has to deal directly with the diffeomorphism together with interpretations return maps along the separatrices like the separatrix map, the standard map, the Arnold map or generalizations (see, e.g., [Broer, Simó and Tatjer, 1998]), in order to get qualitative and quantitative information.

The geometrical point of view adopted along this note becomes a powerful tool to understand birth and death of chaotic dynamics. On the other hand, the numerical strategy followed has allowed us to describe global dynamics and to understand global behaviour and not only local one. Both approximations together are a solid basis to develop an analytic theory for weakly dissipative dynamics (see [Simó and Vieiro, in progress]).

## Acknowledgment

This work has been supported by grants DGI-CYT BFM2003-09504-C02-01 (Spain) and CIRIT 2001SGR-70 (Catalonia). The second author is pleased also to acknowledge support by Ph.D. grant 2003FI00318 (Catalonia).

## References

- Broer, H., Roussarie, R., Simó, C. (1996). Invariant Circles in the Bogdanov-Takens Diffeomorphisms. *Erg. Th. and Dynamical Systems*, **16**, pp. 1147–1172.
- Broer, H., Simó C., Tatjer, J.C. (1998). Towards Global Models Near Homoclinic Tangencies of Dissipative Diffeomorphisms. *Nonlinearity*, **11**, pp. 667–770.
- Dullin, H. R., Meiss, J. D., Sterling, D. (1999). Generic Twistless Bifurcations. *Nonlinearity*, **13**, pp. 203–224.
- Fontich, E., Simó, C. (1990). The Splitting of Separatrices for Analytic Diffeomorphisms. *Erg. Th. and Dynamical Systems*, **10**, pp. 295–318.
- Greene, J. M. (1979). A Method for Computing the

Stochastic Transition. *J. Math. Phys.*, **20**, pp. 1183–1201.

Hénon, M. (1969). Numerical Study of Quadratic Area-Preserving Maps. *Quarterly of applied mathematics*, **3**, vol. **XXVII**, pp. 291–311.

Olvera, A. - Simó, C. (1987) An obstruction method for the destruction of invariant curves. *Physica D*, **26**, pp. 181–192.

Simó, C. (1998). Invariant Curves of Analytic Perturbed Nontwist Area Preserving Maps. *Regular and Chaotic Dynamics*, **3**, pp. 180–195.

Simó, C., Vieiro, A. Planar Radial Weakly-Dissipative Diffeomorphisms: Structure around an Elliptic Point (in progress).